Hindawi
Advances in Civil Engineering
Volume 2022, Article ID 4903650, 17 pages
https://doi.org/10.1155/2022/4903650

Research Article

Investigation on the Effect of Geometric Parameter on Reinforced Concrete Exterior Shear Wall-Slab Connection Using Finite Element Analysis

Aman Hamicha[1] **and Goshu Kenea**[2]

[1]*Civil Engineering Department, College of Engineering and Technology, Bule Hora University, Bule Hora, Oromia, Ethiopia*
[2]*Civil Engineering Department, Jimma Institute of Technology, Jimma University, Jimma, Oromia, Ethiopia*

Correspondence should be addressed to Goshu Kenea; goshukeneatujuba@gmail.com

Received 5 February 2022; Revised 10 March 2022; Accepted 17 March 2022; Published 31 March 2022

Academic Editor: Wonseok Chung

Finite element modeling is becoming widely applicable for the assessment of structural behavior, which is accurate and reliable, since conducting the full experimental test is time-consuming and very expensive. Previously conducted research confirmed that there is a good agreement with the experimental tests. In this study, a nonlinear finite element analysis with the ABAQUS software package has been taken to investigate the response of reinforced concrete exterior shear wall-slab connection subjected to cyclic loading. The structural responses such as load-carrying capacity, energy dissipation, ductility, and stiffness degradation have been studied. Connection type, an aspect ratio of the thickness of the slab to the thickness of the shear wall (t_s/t_w), the aspect ratio of the height of the shear wall to the effective width of the slab (H/W_e), and concrete strength were used as study parameters to evaluate their effect on the structural response of the connection. A total of sixteen models have been selected based on the parametric study and objective of the study. The results show that the exterior shear wall-slab connection with U-type connection has high load-carrying capacity than the other connection types. As the aspect ratios of t_s/t_w, H/W_e and concrete strength increase, the ultimate load capacity and energy dissipation capacity increase. In other words, as the number of loading cycles increases, the stiffness of the connection is decreased.

1. Introduction

In medium and high seismic intensity regions, the structural shear wall has a great role in resisting gravity and lateral loading. Oscillation due to earthquake causes a high-stress concentration with a reverse direction under repetitive loading. During reverse cyclic loading, the structural joints are the most affected area, which may lead to structural failure. The lessons gained from past seismic loads and the research work being carried out in laboratories give a better understanding of the performance of the structure and its components [1].

According to research [2], studies on inelastic static pushover analyses were conducted to investigate the design and capacity evaluation of the shear walls. An overstrength occurred, especially in shear walls with a low height-to-length ratio when compared with the code estimation. The study concluded that the methods in the codes of practice for calculating shear wall capacities need to be improved to achieve economic and safe structures. An experimental investigation [3] was also carried out on the behaviors of the RC frame strengthened with an external shear wall. The test results confirmed that the maximum ultimate lateral load capacity, energy dissipation, and initial rigidity behaviors of the frame strengthened with external shear walls when compared to the bare frames. In addition, a study was performed on the characteristics of slab walls with FE software using the thickness of the slab, materials, and length of the walls as study parameters under both vertical and horizontal loading [4]. The capacity curve was extracted to evaluate the characteristics of the models. Further, an experimental investigation [5] was conducted on the structural

response of two kinds of RC wall-slab connection with anchorage and cross bracings under reversible quasistatic cyclic loading. The results showed that the shear wall-slab connection with anchorage bracing showed higher ductility, higher strength, better energy absorption, and less structural failure related to the shear wall-slab connection with cross-bracing. Based on the study of [6], the seismic response of reinforced concrete exterior wide beam-column connections is investigated through computational simulation using Abaqus. This study is mainly based on the load transfer paths and different performances of the connections with wide and conventional beams. Three-dimensional simulation has been used to model conventional and wide beam-column joints with different beam widths under the influence of quasistatic cyclic loadings. The numerical outputs showed that specimens with wide beam-column connections had lower stiffness and strengths in relation to conventional beam-column joints. The seismic response of buildings is tremendously affected by the rigidity of floors, the arrangement of shear walls, and the connections between the walls and the floors [7].

A research paper [8] with a special form of reinforcement detailing has been conducted to improve the performance of the shear wall-slab connection in terms of ductility and strength under lateral loading. The proposed method can be employed for the design of wall-slab junctions using this special form of reinforcement detailing. In a tall building frame composed of floor slabs and shear walls, the shear wall-slab connection is one of the most significantly stressed areas. The probability of connection damage increases with the increase in the height of a building. According to the finding of [9], they carried out an experimental investigation on an assembled new-type shear wall built with a precast two-way hollow slab. To study its mechanical characteristics, an experimental investigation was conducted on two new-type shear walls and one reinforced concrete shear wall under quasistatic cyclic loading, as the study models. The new-type shear wall specimens with reliable and convenient vertical and horizontal reinforcement are reasonably structured, which leads to sufficient vertical connections force-bearing capacity. The research [10] justified that a very high concentration of flexural, shear, and torsional stresses have occurred at the wall-slab connections when the tall building consisting of coupling slabs and planar walls is subjected to lateral loading. As a reason for their interaction and the stresses concentration, there is a high probability of structural failure to occur at the junction of the shear wall slab. In addition, there is high intensity and nonuniformity of flexural stresses near the periphery of the inner walls. However, the stresses are drastically decreased as we are far away from the wall-slab connection.

On the other hand, different detailing of reinforcement at the joint region has been considered to investigate the seismic response of the shear wall-flat slab connections [11]. The modeling and assessment considered scaled-down exterior wall-slab connection subassemblages to evaluate its response under static reversed cyclic loading. In the study, different reinforcement details were used as study parameters with three-dimensional nonlinear finite element simulations at the joint region using Abaqus/CAE software. In another way, the nonlinear time history analyses were carried out, under different levels of earthquake ground motion, using finite element software computer program Abaqus to investigate the damage mode under seismic loading of the shear wall-slab connection of an RC wall-frame building [12]. Eight-node solid elements have been used to discretize the beams, columns, shear walls, and slabs. Various locations were undertaken and selected to determine the incurred cumulative damage mode in all models. From the investigation, it is confirmed that as the level of ground motion increases, the damage and stresses get highly concentrated at the RC wall-slab connection region.

The shear walls play a primary role in resisting lateral load, in addition to selecting favorable architectural systems, which are normally used at lift shaft or external walls. Most of the time, the lateral load is caused by earthquake loading, wind loading, landslide, and hydrodynamic pressure from a tsunami. However, the connections between shear walls and floor slabs constitute a high potential weak link in shear wall-frame structures to resist the combination of load from vertical and lateral loading. Under the worst load combination, the shear wall-slab connection may have been subjected to a critical stress contour line during sway mode. To avoid the effect of redistribution of loading from wall panel to floor slab, the joints need to be designed with enough percentage of reinforcement and based on the stress concentration at the connection. The study of the behavior of connection between slab and shear wall is of paramount importance in understanding the seismic resistance of slab-wall systems and cyclic loading behavior. To the authors' knowledge, the study conducted on reinforced concrete shear wall-slab connection is very rare. Therefore, this research was concerned with the effect of height of the wall to the width of slab ratio (H/W_e), thickness of the slab to thickness of wall ratio (t_s/t_w), connection type, and concrete grade on an exterior shear wall-slab connection, under cyclic load using finite element analysis. It is focused to investigate the effect of study parameters on ultimate load capacity, energy dissipation capacity, ductility, and the stiffness degradation of the connection under cyclic loading.

2. Summary of Experimental Test for Validation

In this study, the exterior RC shear wall-slab connection with dimensions and detailing reinforcement presented in Figure 1, which was experimentally investigated under cyclic loading [13], was considered to validate the FE simulation. The test specimen was based on one-third scaled-down of full-scale dimension. A conventional detailing reinforcement was employed with a U-type connection. This specimen was denoted by A in the paper. The yield strength of 489.3 N/mm^2 and 458.5 N/mm^2 was employed in the test for 6 mm and 8 mm diameter of steel reinforcement, respectively. The average cubic compressive strength of the concrete was 37.76 MPa. Two steel channels were attached at the

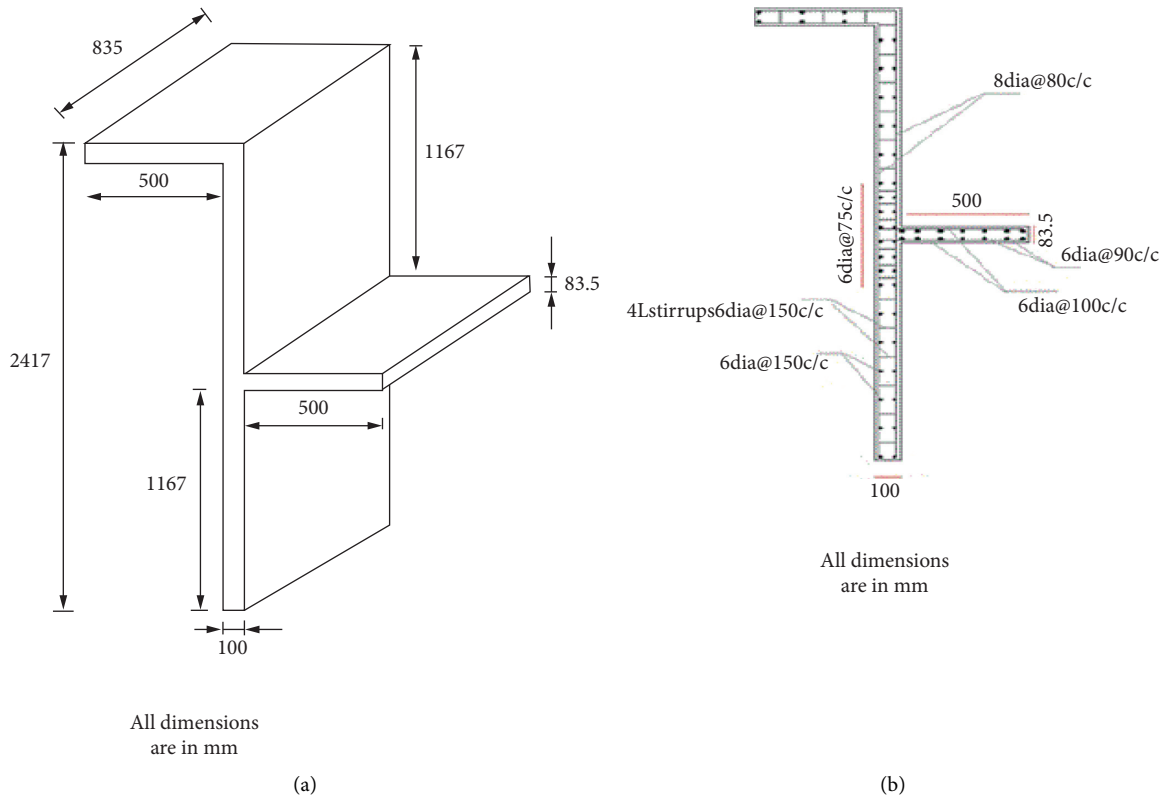

Figure 1: Geometry and detailing of RC shear wall-slab connection from previously conducted experimental work that is used for FE validation [13].

bottom of the shear wall to fix in all directions. An 8 kN weight load was assembled at the top end of the second-floor slab to simulate the axial load. The reverse cyclic loading as illustrated in the research was applied in terms of displacement time history at end of first floor of the slab at both to right and left ends. Detailed information about the test specimen can be obtained from the paper.

3. FE Modeling

3.1. Material Modeling

3.1.1. Concrete

(1) Uniaxial Concrete Compressive Modeling. Concrete uniaxial compressive stress-strain is very important to get compressive damage parameters, which is used as input in FE simulation with the concrete damaged plasticity model. To extract those inputs, different mathematical models may be employed. For this particular study, to obtain uniaxial concrete compressive stress-strain, Eurocode 2 [14] was used as illustrated in (1)–(6). Three concrete cubic compressive strengths with 25 MPa, 30 MPa, and 40 MPa grades were considered to evaluate the effect of concrete strength on the behavior of the model specimens, and one additional concrete grade with 37.76 MPa was used to validate the numerical simulation. Figure 2(a) illustrates the curve between concrete compressive stress and strain, which is linear up to 40% of the ultimate compressive stress [14].

$$\frac{\sigma_c}{f_{\mathrm{cm}}} = \frac{k\eta - \eta^2}{1 + (k-2)\eta}, \tag{1}$$

$$f_{\mathrm{cm}} = f_{ck} + 8\left(\frac{N}{\mathrm{mm}^2}\right), \tag{2}$$

$$k = 1.05E_{\mathrm{cm}}\left(\frac{\varepsilon_{c1}}{f_{\mathrm{cm}}}\right), \tag{3}$$

$$\eta = \frac{\varepsilon_i}{\varepsilon_{c1}}, \tag{4}$$

$$\varepsilon_{c1} = 0.7 f_{\mathrm{cm}}^{0.32} < 2.8, \tag{5}$$

$$E_{\mathrm{cm}} = 22\left[\frac{f_{\mathrm{cm}}}{10}\right]^{0.3}. \tag{6}$$

(2) Uniaxial Concrete Tensile Modeling. Tensile behavior of concrete may have been modeled in terms of stress versus cracking width or strain. The mathematical models proposed in [14] were employed to extract stress-strain input and to compute the ultimate tensile stress of concrete, as presented in (7)–(9). Figure 2(b) shows the tensile stress-strain curve of the concrete. The curve is made from two segments: the first segment is linear with ascending behavior and the second segment is nonlinear with strain softening degradation.

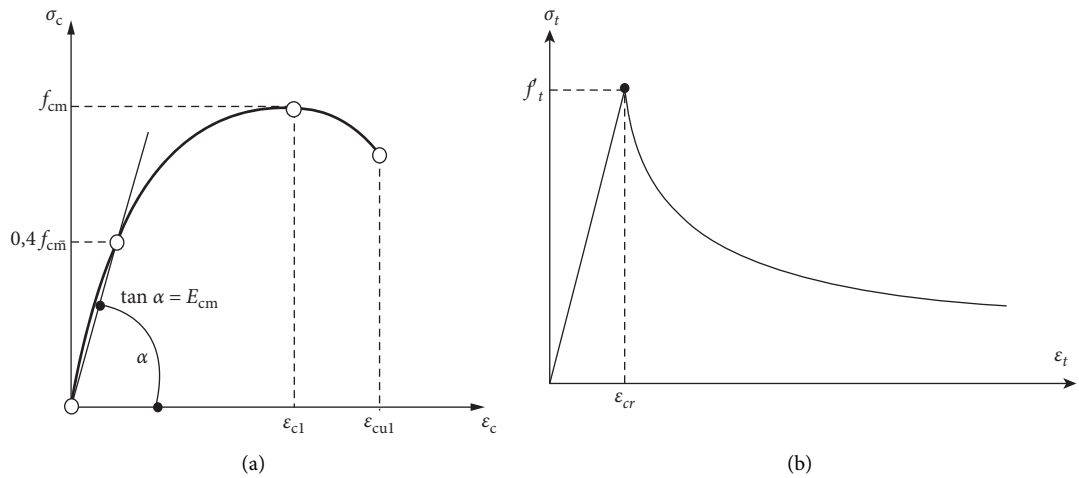

Figure 2: Uniaxial stress-strain of concrete [14]. (a) Compressive stress-strain and (b) tensile stress-strain.

$$f_{ctm} = 0.30 f_{ck}^{(2/3)}, \tag{7}$$

$$\sigma_t = E_t \varepsilon_t, \quad \text{if } \varepsilon_t \le \varepsilon_{cr}, \tag{8}$$

$$\sigma_t = f_{ctm}\left(\frac{\varepsilon_{cr}}{\varepsilon_t}\right)^{0.4}, \quad \text{if } \varepsilon_t \ge \varepsilon_{cr}. \tag{9}$$

(3) Concrete Damage Model. The concrete compressive hardening and tensile stiffening data have been considered in terms of crushing and cracking strain, respectively. The crushing, cracking, and plastic strain (for both compressive and tensile) of concrete has been determined using (10)–(15), as provided in [15–20]. Figures 3(a)–3(d) show the compressive stress-crushing strain, compressive damage-crushing strain, tensile stress-cracking strain, and tensile damage-cracking strain curve of concrete, respectively, under different concrete grades to model the specimens.

$$\sigma_c = (1 - d_c) E_{co}\left(\varepsilon_c - \varepsilon_c^{pl}\right), \tag{10}$$

$$\begin{aligned} \varepsilon_c^{ch} &= \varepsilon_c - \varepsilon_{oc}^{el} \\ &= \varepsilon_c - \frac{\sigma_c}{E_{co}}, \end{aligned} \tag{11}$$

$$\varepsilon_c^{pl} = \varepsilon_c^{ch} - \frac{d_c}{1 - d_c}\frac{\sigma_c}{E_{co}}, \tag{12}$$

$$\sigma_t = (1 - d_t) E_{co}\left(\varepsilon_t - \varepsilon_t^{pl}\right), \tag{13}$$

$$\begin{aligned} \varepsilon_t^{ck} &= \varepsilon_t - \varepsilon_{ot}^{el} \\ &= \varepsilon_t - \frac{\sigma_t}{E_{co}}, \end{aligned} \tag{14}$$

$$\varepsilon_t^{pl} = \varepsilon_t^{cr} - \frac{d_t}{1 - d_t}\frac{\sigma_t}{E_{co}}. \tag{15}$$

(4) Concrete Damage Parameters. The values of concrete damage parameters have been collected from previously conducted investigations [21–26]. The magnitude of each parameter was presented in Table 1.

3.1.2. Steel Reinforcement. The bilinear model [27, 28] was employed for the uniaxial stress-strain response of steel reinforcement. In the adopted skeleton of the stress-strain curve, the first slope of the stress-strain curve represents the elastic modulus, and the second slope represents the hardening modulus of elasticity. The study used steel yield strength of 432 MPa with 0.3 Poisson's ratio and 200 GPa elastic modulus for modeling specimens. In another way, 489.3 N/mm^2 and 458.5 N/mm^2 steel yield strengths were used for validating specimens.

3.2. Geometry, Samples, and Detailed Reinforcement. The paper considered geometric parameter ratio, concrete grade, and connection types as study parameters to investigate the ultimate load capacity, ductility, energy dissipation capacity, and stiffness degradation of reinforced concrete shear wall-slab connection. Based on study parameters, sixteen specimens were selected to cover the objective of the study as illustrated in Table 2, in addition to modeling one validating specimen. The modeling geometry of the RC shear wall-slab connection was scaled down by three as compared to the full-scale geometry dimension. The dimension of the shear wall is constant for all specimens of the study which is given by $(\mathrm{H} * \mathrm{L} * t_w) = 1166.67\,\mathrm{mm} * 600\,\mathrm{mm} * 100\,\mathrm{mm}$. On another hand, slabs having constant 600 mm lengths with different thicknesses and widths were used. Figure 4 and Table 2 show the complete geometric dimension of model specimens. In another way, Table 3 shows the detailed reinforcement of both reinforced concrete shear walls and slab, which is scaled down by three concerning the full-scale detailed reinforcement, which was designed by considering the minimum and maximum reinforcement detailing criteria provided in Eurocode 2 [14] such that it can satisfy ductility requirement.

3.3. Loading and Boundary Conditions. The numerical simulation under consideration was fixed at the bottom to restrict translation and rotation of each element of the shear

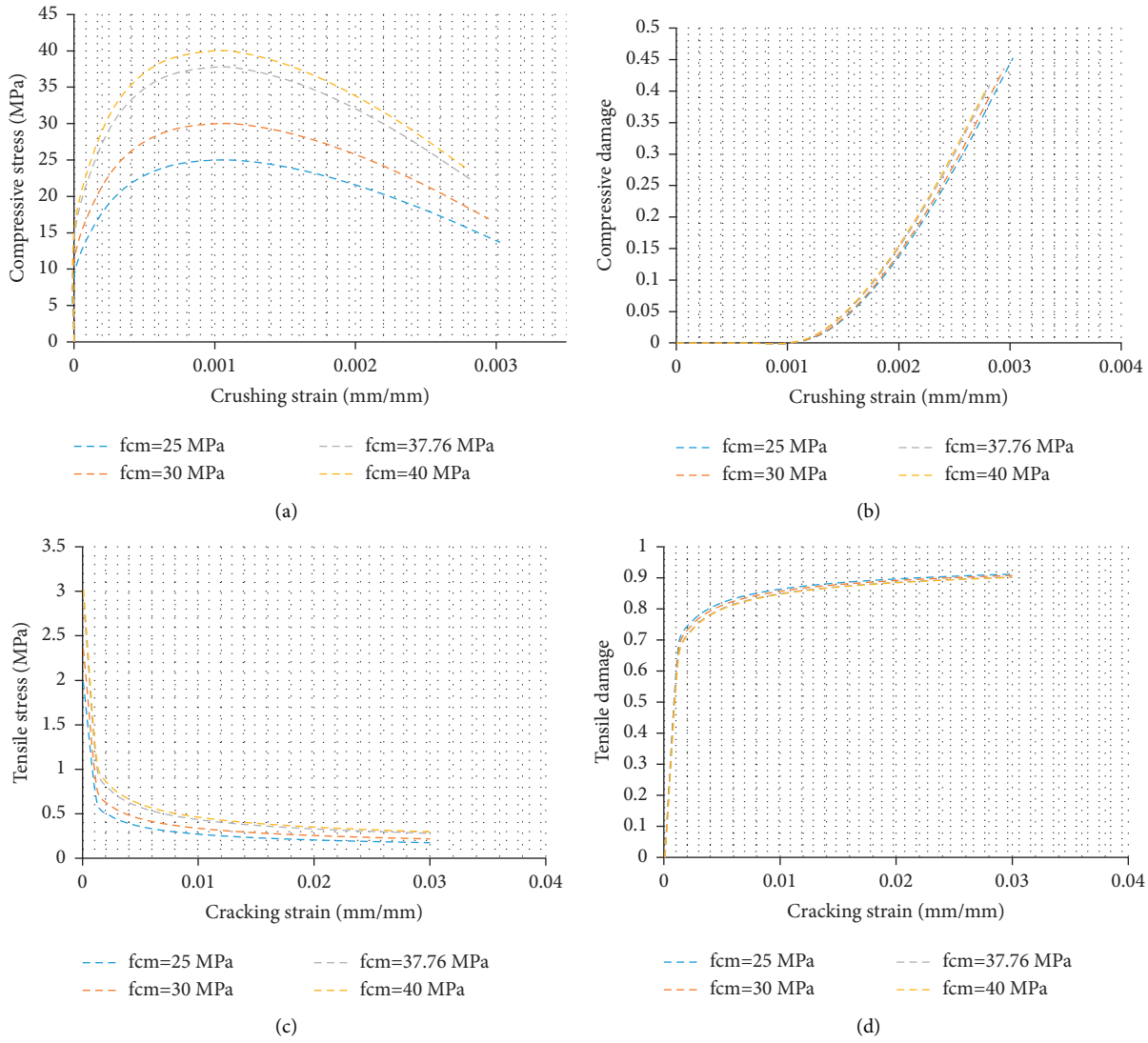

Figure 3: Concrete damage model inputs. (a) Compressive stress versus crushing strain. (b) Compressive damage versus crushing strain. (c) Tensile stress versus cracking strain. (d) Tensile damage versus cracking strain.

Table 1: Concrete damage parameters.

Eccentricity (γ)	Dilation angle (ψ)	K	σ_{bo}/σ_{co}	Viscosity parameter
0.1	38	0.667	1.16	0.001

Table 2: Number of specimens used in FE modeling based on the study parameters.

Specimen	t_s	t_w	H	W_e	t_s/t_w	H/W_e	Connection type	Concrete (MPa)
C1SWS1	60	100	1166.67	700	0.6	1.67	U-type	30
C1SWS2	80	100	1166.67	700	0.8	1.67	U-type	30
C1SWS3	100	100	1166.67	700	1.0	1.67	U-type	30
C2SWS1	60	100	1166.67	700	0.6	1.67	90°-type	30
C2SWS2	80	100	1166.67	700	0.8	1.67	90°-type	30
C2SWS3	100	100	1166.67	700	1.0	1.67	90°-type	30
C3SWS1	60	100	1166.67	700	0.6	1.67	135°-type	30
C3SWS2	80	100	1166.67	700	0.8	1.67	135°-type	30
C3SWS3	100	100	1166.67	700	1.0	1.67	135°-type	30
C4SWS1	60	100	1166.67	700	0.6	1.67	150° type	30
C4SWS2	80	100	1166.67	700	0.8	1.67	150° type	30

Table 2: Continued.

Specimen	t_s	t_w	H	W_e	t_s/t_w	H/W_e	Connection type	Concrete (MPa)
C4SWS3	100	100	1166.67	700	1,0	1.67	150° type	30
C1SWS1-1	60	100	1166.67	800	0.6	1.46	U-type	30
C1SWS1-2	60	100	1166.67	900	0.6	1.3	U-type	30
C1SWS1-3	60	100	1166.67	700	0.6	1.67	U-type	25
C1SWS1-4	60	100	1166.67	700	0.6	1.67	U-type	40

t_s: thickness of slab; t_w: thickness of wall; H: height of wall; W_e: width of slab.

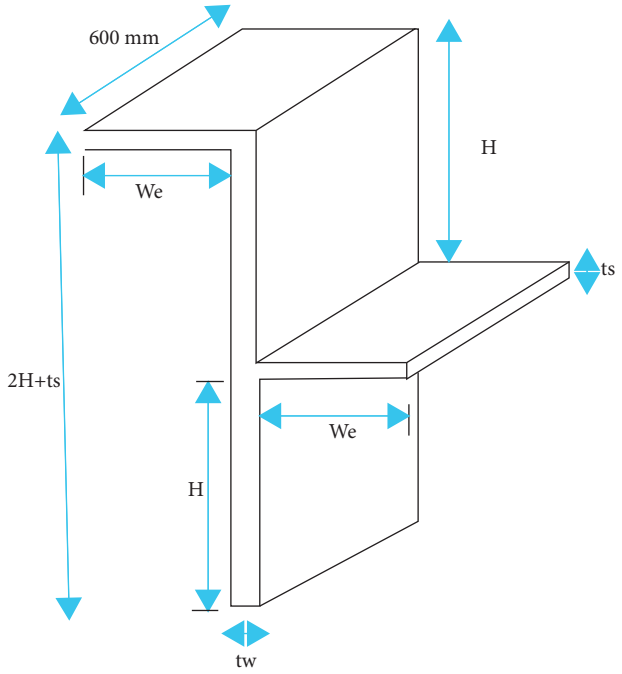

Figure 4: Geometric dimension of model specimens.

wall for all degrees of freedom and to reflect the behavior of the shear wall used for the experimental study. The top of the shear wall was restrained against in-plane and out-of-plane movement by employing roller support. The axial load (8 kN) at the top of the subassembly was distributed as a pressure on the top face of the model to simulate axial load. Using two circular partition profiles, a 25 mm displacement was applied on the left and right end of the first floor slab with the cyclic amplitude time history provided in Figure 5. In other cases, 8 mm displacement was applied for validating the specimen. This cyclic amplitude time history was obtained from the displacement time history provided in [13]. Figure 6 illustrates the loading and boundary conditions of the model specimen.

3.4. Meshing Size and Element Types. The meshing size of all the parts in the models was determined to be 50 mm for both concrete and steel bar after several iterations until the result of FE simulation result becomes constant. An 8-node linear brick, hourglass control, reduced integration (C3D8R) and a 2-node linear 3D truss (T3D2) were used to model concrete and steel bar, respectively, as shown in Figure 7.

4. Validation of FE Modeling

Before moving to the study modeling and simulation, validation has been conducted against previously published experimental investigation [13]. To capture the cyclic behavior of exterior shear wall-slab connection, a lot of parameters have been considered in this study. Some of the things are a nonlinear material model for steel and concrete, using different loading rates (amplitude), boundary conditions, mesh size, and element type. The selected model captures accurately, the failure mode, the deformation, and the lateral load capacity of the exterior shear wall-slab connection as compared to the experimental result. Because of the pinching behavior of reinforced concrete, the hysteresis curve of finite element analysis cannot capture the exact behavior of the hysteresis curve of experimental around the origin. In reinforced concrete, pinching is typically produced by the opening of cracks when displacement is imposed in one direction. Partial stiffness recovery occurs when cracks are closed during displacements imposed in the other direction. Therefore, instead of the hysteresis curve, the envelope curve was used to compare FE and experimental results, as illustrated in Figure 8(a). Table 4 shows the ultimate load capacity obtained from FE analysis and experimental investigation with a 3.704% difference. In addition, the deformation of the RC shear wall-slab joint obtained from the FE simulation was presented in Figure 8(b) with a very small difference, when compared to experimental deformation. Furthermore, the comparison between FE and the experimental result was assessed in terms of failure mode. The failure mode happened almost in a similar way with the experimental investigation, in which cracking occurred at an inclined angle to the edge of the slab, as shown in Figure 9. All results showed a good agreement between FE analysis and experimental test.

5. Parametric Study

5.1. Ultimate Load Capacity

5.1.1. Effect of Aspect Ratio (t_s/t_w). A sophisticated FE analysis has been conducted in Abaqus software, in which different parameters are considered to assess its effect on the ultimate capacity of the shear wall-slab connection. Aspect ratio (t_s/t_w) was undertaken as one parameter to investigate the ultimate capacity of shear wall-slab connection keeping other parameters constant for different types of connection. Figure 10(a) shows the ultimate load capacity of the shear wall-slab connection with U-type connection by considering

Table 3: Detailing for both reinforced concrete slab and shear wall for the connections.

No.	Denoted by	Slab reinforcement		Shear wall reinforcement		
		Longitudinal	Transverse	Vertical	Horizontal	Stirrups
1	C1SWS1	ϕ4 mm@96 mm	ϕ4mm@96 mm	Ø6c/c 90 mm vertical bar on both faces of shear wall	Ø4c/c 130 mm horizontal bar on both faces of shear wall	Ø2mmc/c 130 mm
2	C1SWS2	ϕ4 mm@70 mm	ϕ4mm@66 mm			
3	C1SWS3	ϕ4 mm@53 mm	ϕ4mm@53 mm			
4	C2SWS1	ϕ4 mm@96 mm	ϕ4mm@93 mm			
5	C2SWS2	ϕ4 mm@70 mm	ϕ4 mm@66 mm			
6	C2SWS3	ϕ4 mm@53 mm	ϕ4 mm@53 mm			
7	C3SWS1	ϕ4 mm@96 mm	ϕ4 mm@93 mm			
8	C3SWS2	ϕ4 mm@70 mm	ϕ4mm@66 mm			
9	C3SWS3	ϕ4 mm@50 mm	ϕ4 mm@50 mm			
10	C4SWS1	ϕ4 mm@96 mm	ϕ4 mm@93 mm			
11	C4SWS2	ϕ4 mm@70 mm	ϕ4 mm@66 mm			
12	C4SWS3	ϕ4mm@50 mm	ϕ4mm@50 mm			
13	C1SWS1-1	ϕ4 mm@96 mm	ϕ4 mm@96 mm			
14	C1SWS1-2	ϕ4 mm@96 mm	ϕ4 mm@96 mm			
15	C1SWS1-3	ϕ4 mm@96 mm	ϕ4 mm@96 mm			
16	C1SWS1-4	ϕ4 mm@96 mm	ϕ4 mm@96 mm			

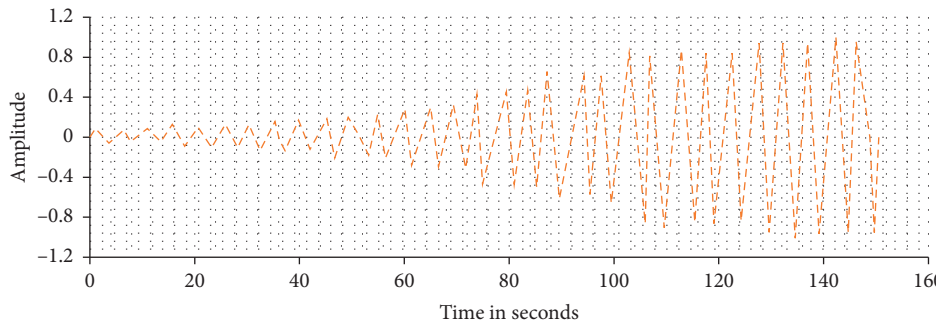

Figure 5: Amplitude time history to apply cyclic loading.

different thicknesses of the slab to the thickness of shear wall ratio. The aspect ratio (t_s/t_w) has a significant effect on the ultimate resistance of the shear wall-slab connection. As the aspect ratio increased from 0.6 to 0.8 and from 0.8 to 1.0, the ultimate load capacity increased by 61.17% and 73.36%, respectively. This implies that, as the aspect ratio increases, the performance of the connection is increased under cyclic loading. Additionally, the ultimate capacity of the connection has been studied with a 90°-type connection under different aspect ratios (t_s/t_w). Figure 10(b) presents the ultimate capacity of the shear wall-slab connection with a 90°-type connection under different aspect ratios. As the aspect ratio increased from 0.6 to 0.8 and from 0.8 to 1.0, the ultimate load capacity increases by 61.49% and 71.86%, respectively. Further, the connection was modeled with a 135°-type connection to evaluate the ultimate capacity of the shear wall-slab connection by considering different aspect ratios.

Figure 10(c) illustrates the effect of aspect ratio (t_s/t_w) on the capacity shear wall-slab connection with 135°-type of connection. As the aspect ratio increased from 0.6 to 0.8 and from 0.8 to 1.0, the ultimate load capacity increased by 61.64% and 72.35%, respectively. Furthermore, the effect of aspect ratio was studied on the ultimate capacity of the joints with 150° type of connection. The result obtained from finite element simulation was presented in Figure 10(d) to assess the effect aspect ratio with 150° type of connection. The ultimate resistance of the connection increased by 61.43% and 72.49%, as the aspect ratio increases from 0.6 to 0.8 and from 0.8 to 1.0, respectively. This all shows that the aspect ratio (t_s/t_w) has an extreme effect on the ultimate resistance of the shear wall-slab connection. The shear wall-slab connection with a larger aspect ratio has a good performance under cyclic loading.

5.1.2. Effect of Aspect Ratio of (H/W_e). The study also considered the effect of aspect ratio (H/W_e) on the load resisting capacity of the reinforced concrete shear wall-slab connection. Figure 11 describes the results of the load-carrying capacity of the connection with a different aspect ratio (H/W_e), keeping other parameters constant. As understood from the result, the aspect ratio (H/W_e) slightly affects the ultimate capacity of the connection when compared to (t_s/t_w) ratio. Three aspect ratios (H/W_e) with a magnitude of 1.67, 1.46, and 1.30 were considered for the study. The study indicated that the ultimate load capacity of the shear wall-slab connection decreased as the effective

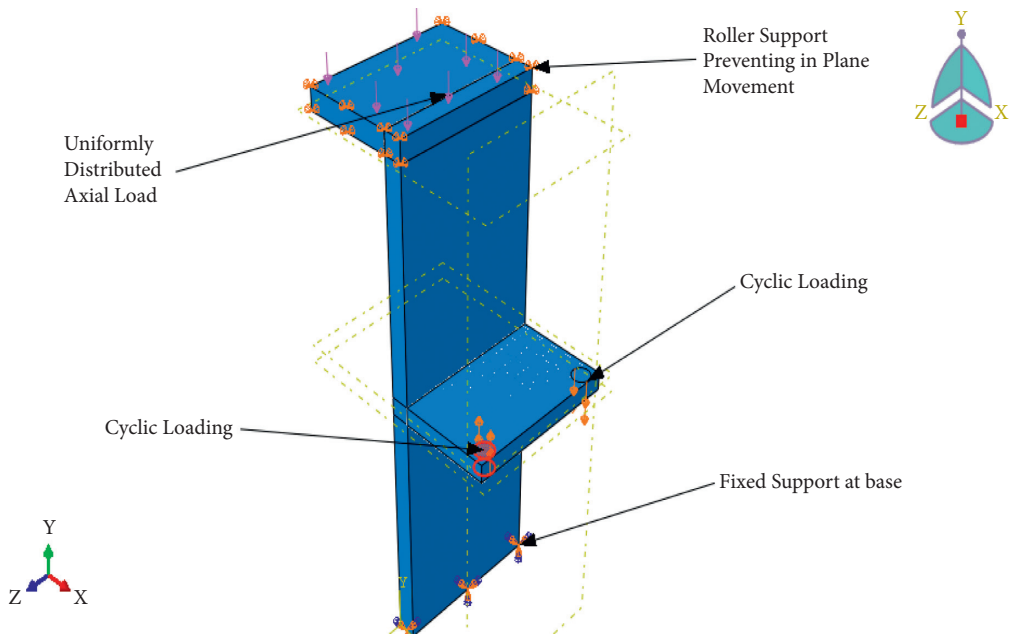

Figure 6: Boundary and loading condition of the models.

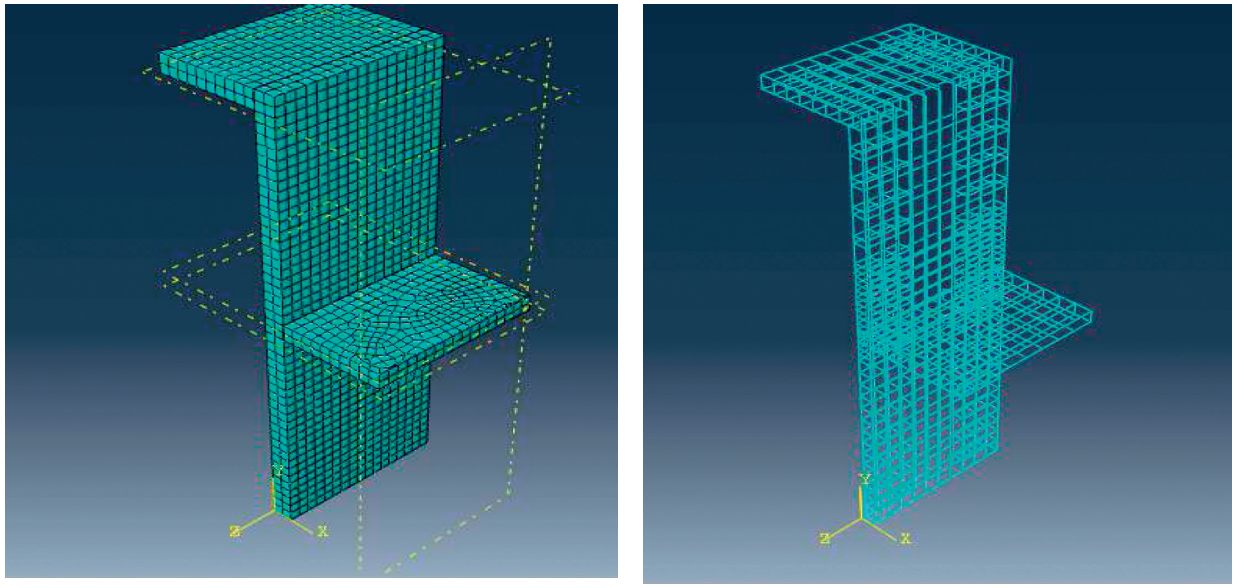

(a) (b)

Figure 7: Meshing size and element type for each part of shear wall-slab connection. (a) Plain concrete shear wall-slab joint and (b) steel reinforcement.

width of the slab increased (H/W_e ratio decreased). The ultimate load resistance of the connection with an aspect ratio (H/W_e) of 1.67 was 1.15% and 1.6% greater than the connection with an aspect ratio (H/W_e) of 1.46 and 1.3, respectively. In general, the connection with the larger aspect (H/W_e) ratio has a good performance under cyclic loading.

5.1.3. Effects of Connection Type. The type of connection was also undertaken as a study parameter to investigate its effect on the ultimate resistance of the RC shear wall-slab connection. The four types of connection undertaken include U-type connection, 90°-type connection, 135°-type connection, and 150°-type connection. Their effect was investigated by keeping other parameters constant. Figure 12 indicates the effect of connection type on the ultimate load capacity of the connections under cyclic loading. The result confirmed that the specimen with a U-type connection showed a better performance than the other connection types. The ultimate resistance of the shear wall-slab connection with U-type connection is 0.621%, 0.336%, and 0.267% greater than the shear wall-slab connection with 90°-

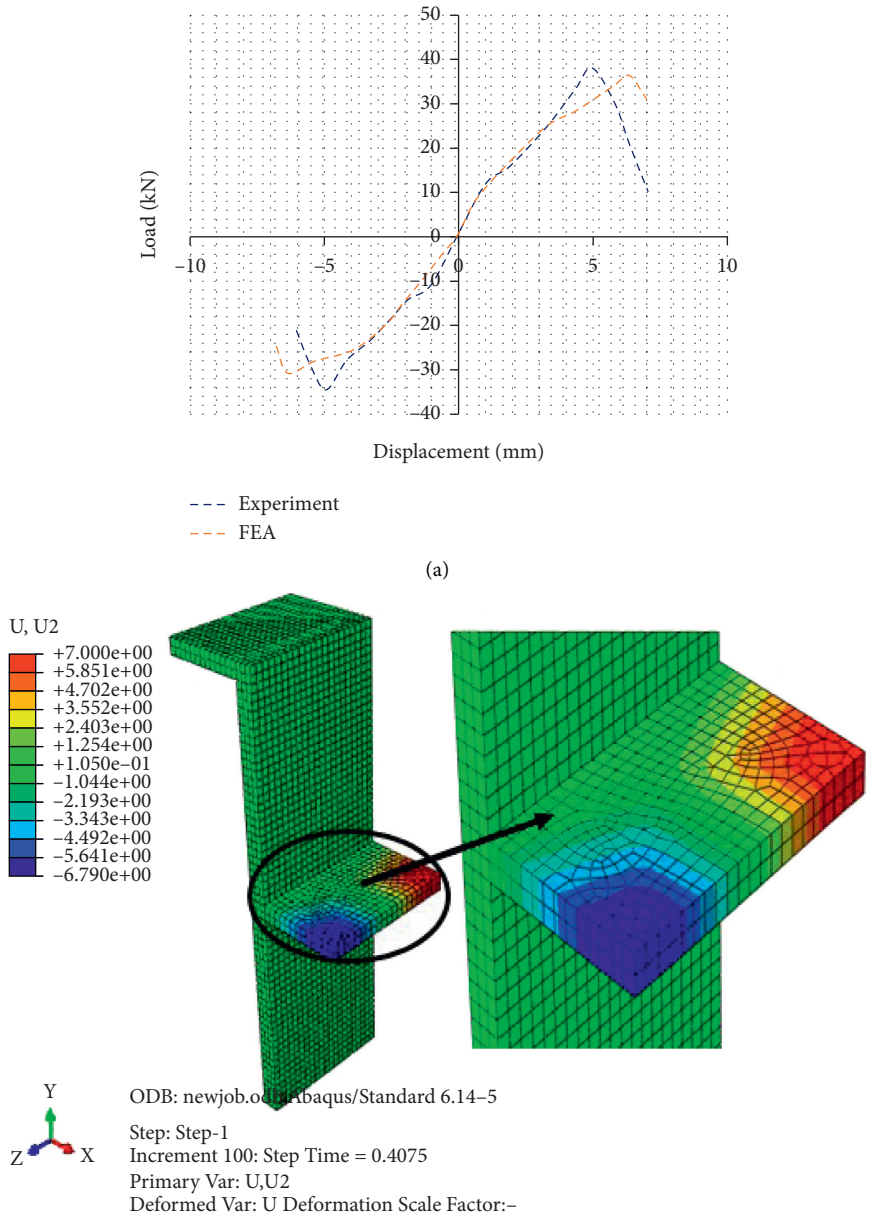

Figure 8: Comparison of experimental [13] and finite element results.

Table 4: Comparison of FE analysis and experimental result.

Source	Variable	FE result (kN)	Experimental result (kN)	Difference	Percentage difference (%)
[13]	P_{ult}	36.38	37.8	1.40	3.704

P_{ult}: ultimate load capacity.

type connection, 135°-type connection, and 150°-type connection, respectively. This implies that the connection type slightly affects the ultimate capacity of the connection. Therefore, the cyclic loading performance of shear wall-slab connection with U-type connection is slightly greater than other types of connections.

5.1.4. Effects of Concrete Grade. Figure 13 describes the results of the ultimate load capacity of the reinforced concrete shear wall-slab connection by considering the different concrete grades. Three concrete compressive strengths with a magnitude of 25 MPa, 30 MPa, and 40 MPa were considered for the investigation. The result from the FE simulation

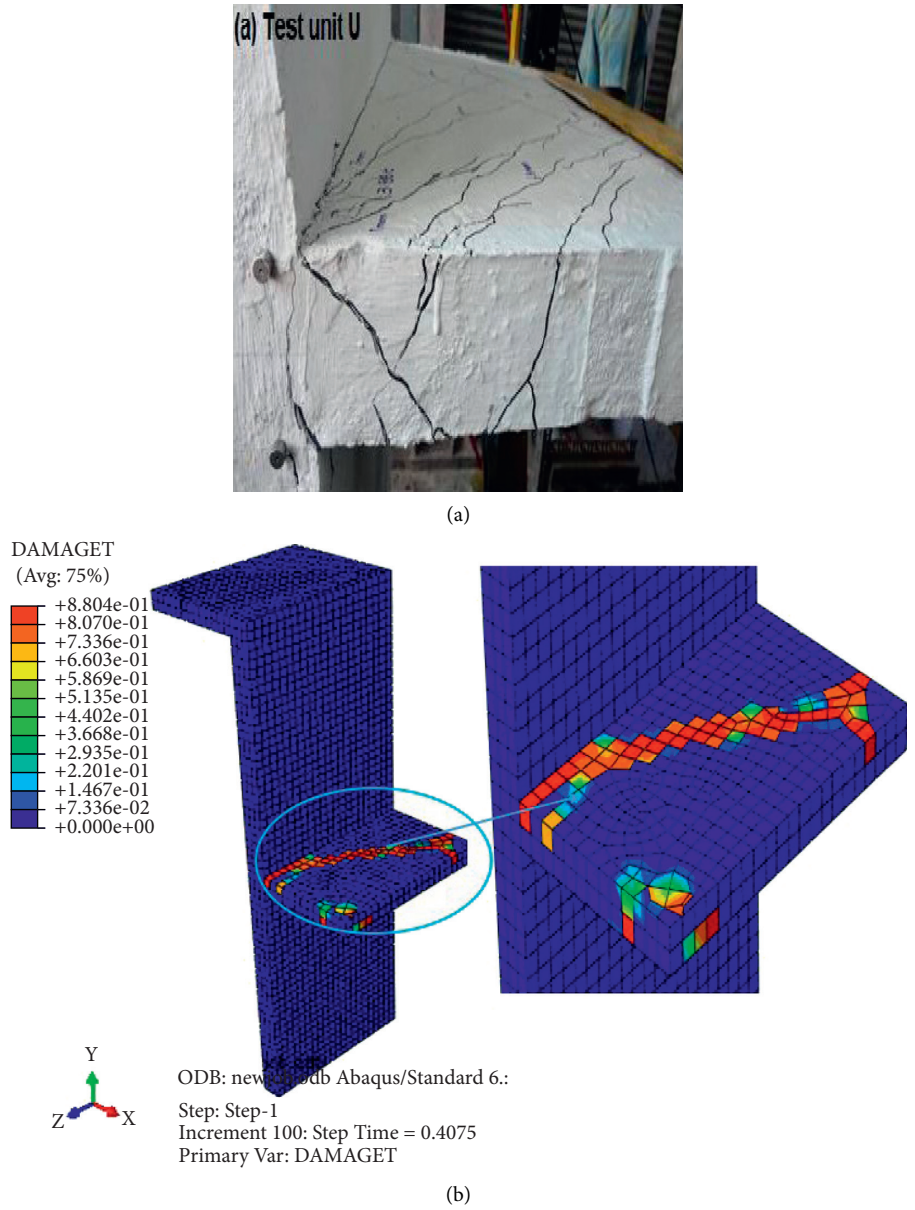

Figure 9: Comparison of damage mode for experimental and FE model results.

confirmed the significant effect of concrete grade on the shear wall-slab connection under cyclic loading. With the increase of concrete compressive strength, the ultimate load capacity of the shear wall-slab connection also increases. As the concrete grade increased from C-25 MPa to 40 MPa and C-30 MPa to C-40 MPa, the ultimate load resistance of the shear wall-slab connection was increased by 31.28% and 25.94%, respectively. Therefore, the connection with higher concrete grade has a good performance under cyclic loading.

5.2. Energy Dissipation and Damping Ratio. The inelastic deformation of shear wall-slab connections helps to dissipate a sufficient amount of energy through hysteretic behavior, thereby reducing the energy transmission and ensuring that a structure performs satisfactorily in the event of a strong earthquake. The cumulative energy dissipation and equivalent viscous damping ratio are important indicators and are calculated based on the hysteretic loops. The amount of dissipated energy at each cycle is calculated as the sum of the areas enclosed by the load-displacement hysteresis loops [29]. The cumulative energy dissipation is expressed as the sum of the energy dissipation. The equivalent viscous damping ratio (h_e) was computed using

$$\text{Damping ratio}\,(h_e) = \frac{S_{AEBF}}{2\pi\left(S_{OAD} + S_{OBC}\right)}, \tag{16}$$

where S_{AEBF} is the area of the enclosed curve and is computed by using origin lab software and S_{OAD} and S_{OBC} are the areas of OAD and OBC sections of the curve, respectively, as illustrated in Figure 14.

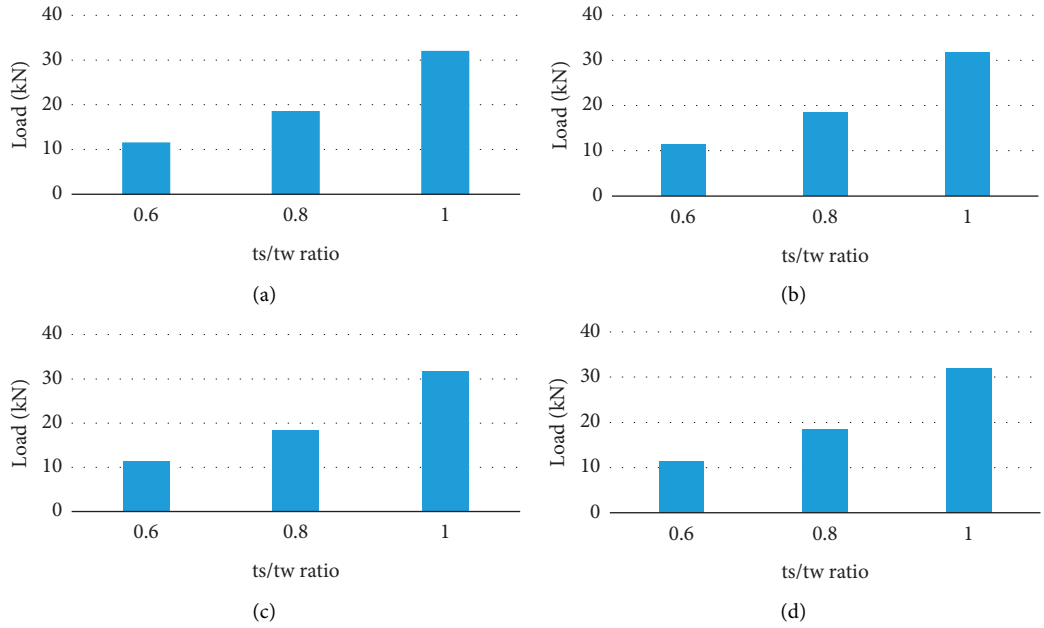

Figure 10: Effect of aspect ratio (t_s/t_w) on ultimate capacity of the joint with different connections. (a) U-type, (b) 90°-type, (c) 135°-type, and (d) 150°-type connection.

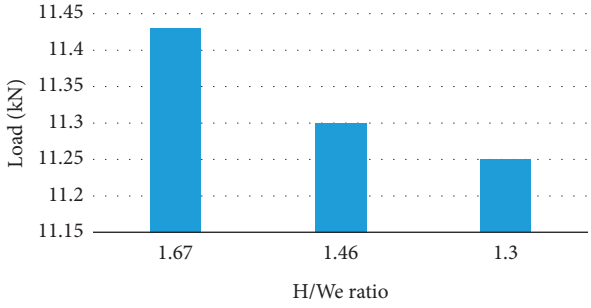

Figure 11: Effect of aspect ratio (H/W_e) on the ultimate load capacity of the connection.

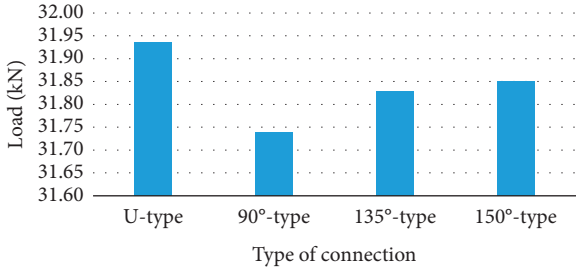

Figure 12: Effect of type of connection on the ultimate load capacity of the connection with t_s/t_w equal to 1.

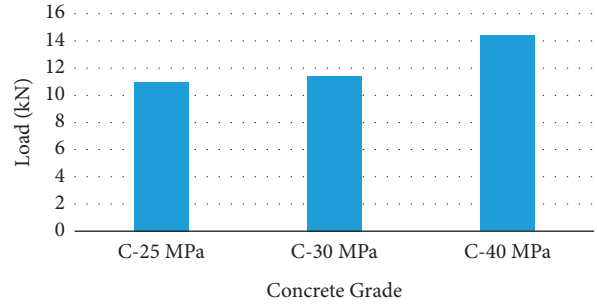

Figure 13: Effect of concrete strength on the ultimate load capacity with U-type connection.

5.2.1. Effect of Aspect Ratio (t_s/t_w)

(1) U-Type Connection. The cumulative energy dissipation capacity was increased by 17.7%, as the aspect ratio (t_s/t_w) increased from 0.6 to 0.8. On other hand, as the aspect ratio (t_s/t_w) increased from 0.6 to 1.0, the cumulative energy dissipation capacity increased by 128.83%. This implies that the cumulative energy dissipation capacity is significantly affected by the aspect ratio (t_s/t_w). Table 5 shows the cumulative energy dissipation and viscous damping ratio of shear wall-slab connection with U-type connection under different aspect ratios (t_s/t_w).

(2) 90°-Type Connection. The cumulative energy dissipation capacity of the connection with an aspect ratio (t_s/t_w) with 0.8 and 1.0 was increased by 15.61% and 118.74%, respectively, when compared to the connection with an aspect ratio (t_s/t_w) of 0.6. Table 6 presents the cumulative energy dissipation capacity and equivalent viscous damping ratio of the shear wall-slab connection with the 90°-type connection under different aspect ratios (t_s/t_w).

(3) 135°-Type Connection. As aspect ratio (t_s/t_w) increased from 0.6 to 0.8 and from 0.6 to 1.0, the cumulative energy dissipation capacity increased by 16.46% and 131.66%, respectively, when 135°-type connection was used. Table 7 presents the cumulative energy dissipation capacity and

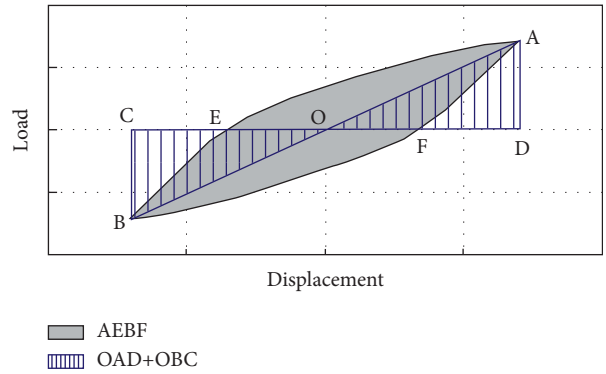

Figure 14: Definition of energy dissipation and equivalent viscous damping ratio [29].

equivalent viscous damping ratio with a 135°-type connection.

(4) 150°-Type Connection. As aspect ratio (t_s/t_w) increased from 0.6 to 0.8 and 0.6 to 1.0, the cumulative energy dissipation capacity increased by 14.6% and 134.49%, respectively, with 150°-type connection. Table 8 presents the cumulative energy dissipation capacity and equivalent viscous damping ratio with a 150°-type connection.

5.2.2. Effect of Aspect Ratio (H/W_e). The effect of aspect ratio (H/W_e) on cumulative energy dissipation and damping ratio was also accessed as shown in Table 9. It is confirmed that as the effective width of the slab increased in the exterior shear wall-slab connection, the ability of the connection to absorb the cumulative energy was decreased. The specimen with an aspect ratio of H/W_e of 1.67 absorbs cumulative energy of 76.35% more than the aspect ratio of H/W_e of 1.46 and 106.70% more than the aspect ratio of 1.30.

5.2.3. Effects of Connection Type. Based on the result presented in Table 10, the cumulative dissipation energy is slightly affected by types of connection when compared to other study parameters. The result showed that the specimen with a 150°-type connection showed a better performance than the other connections. The 150°-type connection specimen exhibited the cumulative energy dissipation capacity that is 0.89% greater than the U-type connection, 4.9% greater than the 90°-type connection, and 0.73% greater than the 135°-type connection specimen under the same conditions.

5.2.4. Effects of Concrete Grade. Table 11 shows the cumulative dissipation energy of the models with different concrete strengths. The energy that was absorbed in the model with a concrete grade of C-40 MPa was 39.46% than the model with C-25 MPa and 17.90% than the model with a concrete grade of C-30 MPa. With respect to these values, it was concluded that the amount of energy absorbed was increased as concrete grade increased.

5.3. Displacement Ductility Factor. Ductility is defined as the ability of a structure and its elements to resist huge inelastic deformation without any significant reduction in strength. Ductile structures have the capability of dissipating hysterically large magnitude of energy during the inelastic cyclic deformations. A displacement ductility factor is computed as the ratio of the displacement at ultimate to the displacement at yield according to equation (17). In this study, the ductility of RC shear wall-slab slab connection calculation based on simplification method presented in Figure 15. The load-displacement relation may not lead to a well-defined yield point due either to the nonlinear behavior of the materials or to the onset of yield at different load levels in different structural components. This leads to a somewhat subjective determination of yielding deformation in reinforced concrete structures. Envelope curves were obtained by joining the peak points of all the cycles. Using these envelopes, ductility factors for the specimens were obtained. For each model, the load-displacement envelope was used to define the yield and maximum displacements following the method used by [30]. Figure 16 illustrates the envelope curve of the RC shear wall-slab connection under cyclic loading.

$$Dultilit\,y\,(\mu) = \frac{\Delta_u}{\Delta_y}. \tag{17}$$

From the analysis, it can be concluded that as the aspect ratio (t_s/t_w) increases for the same connection, the ductility of the RC exterior shear wall-slab connection tends to increase. Table 12 presents the summary of output from FE simulation, and it was concluded that the specimen denoted with C3SWS3 was more ductile than the other specimens.

5.4. Stiffness Degradation. In the case of reinforced concrete shear wall-slab connection, stiffness of the joint gets reduced when the joint is subjected to cyclic/repeated/dynamic loading. This reduction in stiffness is due to loading, unloading, and reloading processes. This will cause the initiation of microcracks inside the joint and will sometimes lead to the fatigue limit of the materials. This, in turn, increases the deformations inside the joints, thus resulting in a reduction in stiffness. Hence, it is necessary

Table 5: Cumulative energy dissipation and viscous damping ratio of U-type connection.

Specimen designation	Area of OAD Positive (kN mm)	Area of OBC Negative (kN mm)	$2 * \pi * (S_{OAD} + S_{OBC})$ (kN mm)	Area of Loop (kN mm)	h_e
C1SWS1	131.490	134.719	1671.793	1331.143	0.80
C1SWS2	145.480	146.214	1831.839	1566.701	0.86
C1SWS3	248.959	250.449	3136.285	3046.029	0.97

Table 6: Cumulative energy dissipation and viscous damping ratio of 90°-type connection.

Specimen designation	Area of OAD Positive (kN mm)	Area of OBC Negative (kN mm)	$2 * \pi * (S_{OAD} + S_{OBC})$ (kN mm)	Area of Loop (kN mm)	h_e
C2SWS1	132.079	134.503	1674.131	1339.000	0.80
C2SWS2	145.847	146.623	1836.709	1548.0000	0.84
C2SWS3	243.516	249.271	3094.702	2929.000	0.95

Table 7: Cumulative energy dissipation and viscous damping ratio of 135°-type connection.

Specimen designation	Area of OAD Positive (kN mm)	Area of OBC Negative (kN mm)	$2 * \pi * (S_{OAD} + S_{OBC})$ (kN mm)	Area of Loop (kN mm)	h_e
C3SWS1	131.492	133.862	1666.421	1316.800	0.79
C3SWS2	145.811	146.669	1836.777	1533.541	0.83
C3SWS3	247.403	249.383	3119.814	3050.471	0.98

Table 8: Cumulative energy dissipation and viscous damping ratio of 150°-type connection.

Specimen designation	Area of OAD Positive (kN mm)	Area of OBC Negative (kN mm)	$2 * \pi * (S_{OAD} + S_{OBC})$ (kN mm)	Area of Loop (kN mm)	h_e
C4SWS1	132.178	133.955	1671.311	1310.346	0.78
C4SWS2	145.926	146.450	1836122	1501.657	0.82
C4SWS3	247.403	251.583	3133.632	3072.68	0.98

Table 9: Cumulative energy dissipation and EVD for aspect ratio of H/W_e.

Specimen designation	Area of OAD Positive (kN mm)	Area of OBC Negative (kN mm)	$2 * \pi * (S_{OAD} + S_{OBC})$ (kN mm)	Area of Loop (kN mm)	h_e
C1SWS1	131.490	134.719	1671.793	1331.143	0.80
C1SWS1-1	88.066	85.184	1088.006	754.847	0.69
C1SWS1-2	90.410	91.978	1145.396	643.984	0.56

Table 10: Cumulative energy dissipation and EVD of connection type.

Specimen designation	Area of OAD Positive (kN mm)	Area of OBC Negative (kN mm)	$2 * \pi * (S_{OAD} + S_{OBC})$ (kN mm)	Area of Loop (kN mm)	h_e
C1SWS3	248.959	250.449	3136.285	3046.029	0.97
C2SWS3	243.516	249.271	3094.702	2929.000	0.95
C3SWS3	247.403	249.383	3119.814	3050.471	0.98
C4SWS3	247.403	251.583	3133.632	3072.680	0.98

Table 11: Cumulative energy dissipation and viscous damping ratio for grade of concrete.

Specimen designation	Area of OAD Positive (kN mm)	Area of OBC Negative (kN mm)	$2 * \pi * (S_{OAD} + S_{OBC})$ (kN mm)	Area of Loop (kN mm)	h_e
C1SWS1-3	125.932	130.675	1611.493	1125.436	0.69
C1SWS1	132.178	133.960	1671.347	1331.143	0.79
C1SWS1-4	122.405	145.570	1682.882	1569.476	0.93

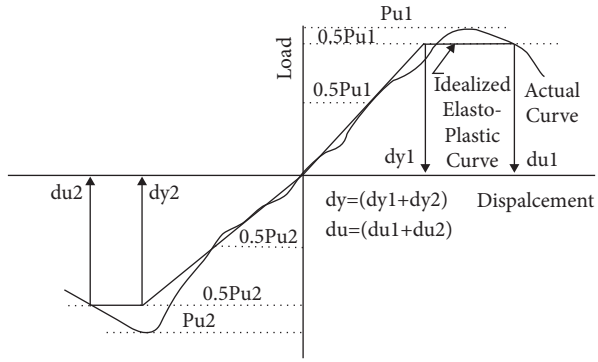

Figure 15: Method used to define the yield and ultimate displacements [30].

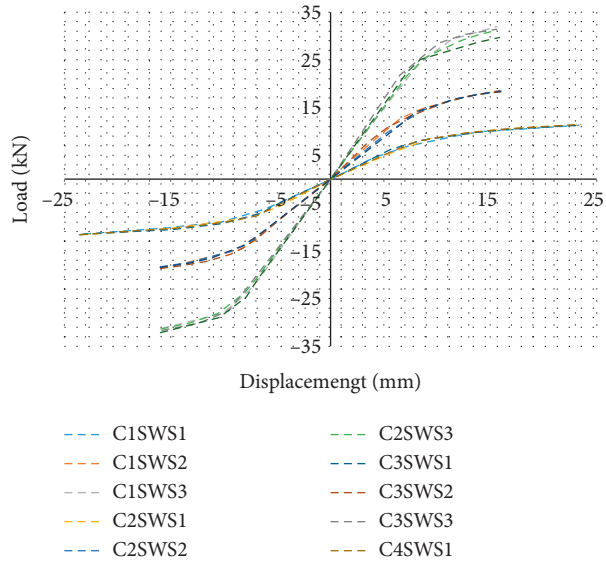

Figure 16: Comparison of load-displacement envelope curves of the model specimens.

Table 12: Summary of displacement and load at yield and ultimate for different specimens.

Specimen designation	Yield load (kN)	Displacement at yield load (mm) Δ_y	Ultimate load (kN)	Displacement at ultimate load (mm) Δ_u	Ductility factor $\mu = (\Delta_u/\Delta_y)$
C1SWS1	6.93	10.5	11.40	23.31	2.22
C1SWS2	12.77	6.60	18.64	15.95	2.42
C1SWS3	24.39	6.45	31.63	15.76	2.44
C2SWS1	8.50	9.92	11.51	23.47	2.36
C2SWS2	14.34	6.53	18.43	16.03	2.45
C2SWS3	21.72	6.37	31.40	15.96	2.51
C3SWS1	6.23	9.2	11.42	23.47	2.55
C3SWS2	10.93	5.56	18.51	16.06	2.89
C3SWS3	21.81	5.36	31.56	15.75	2.94
C4SWS1	7.93	11.87	11.56	23.59	1.98
C4SWS2	14.08	8.01	18.43	16.03	2.00
C4SWS3	22.40	7.18	30.93	15.96	2.22
C1SWS1-1	6.85	11.01	11.30	25.10	2.28
C1SWS1-2	6.82	11.43	11.25	26.40	2.31
C1SWS1-3	5.98	11.49	10.97	27.00	2.35
C1SWS1-4	8.73	10.01	14.41	21.92	2.19

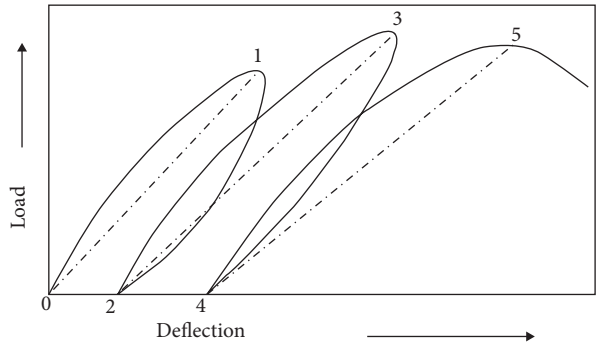

Figure 17: The procedure adopted for determining secant stiffness [31].

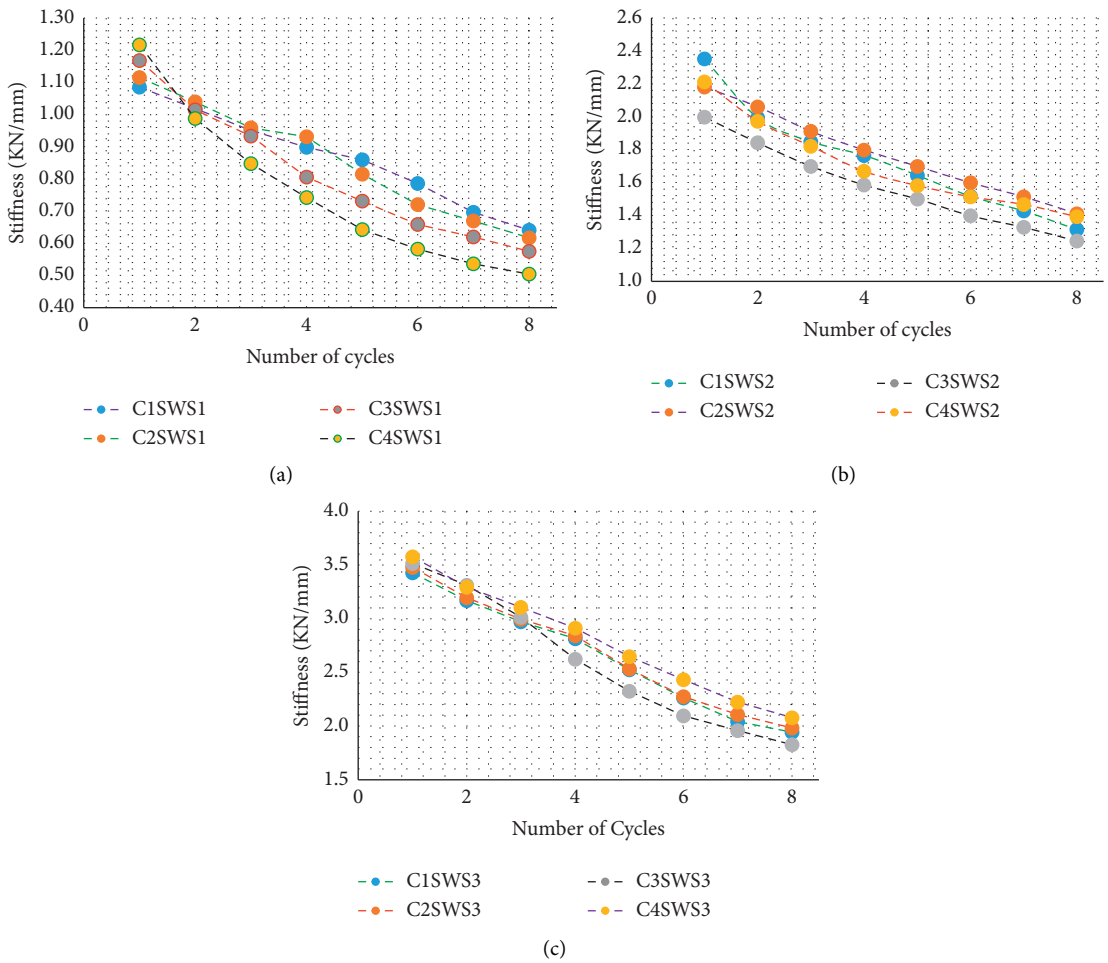

Figure 18: Effect of connection types on the stiffness degradation for aspect ratio (t_s/t_w).

to evaluate the degradation of stiffness in the shear wall-slab joints subjected to cyclic or repeated loading. To determine the degradation of stiffness, Figure 17 was used as proposed in [30].

The values of the secant stiffness were computed from each loading cycle to evaluate the stiffness degradation. Figures 18(a), 10(b), and 10(c) illustrate the stiffness degradation of the RC shear wall-slab connection with different types of connection with an aspect ratio (t_s/t_w) equal to 0.6, 0.8, and 1.0, respectively. In general, as the number of loading cycles increases, the stiffness of the specimen decreases.

6. Conclusion

An investigation was conducted on a reinforced concrete exterior shear wall-slab connection based on different thickness of the slab to thickness of the shear wall (t_s/t_w) the

height of the shear wall to the effective width of slab (H/W_e) ratio, concrete strength, and connection types as study parameters to see their effects on the ultimate load capacity, energy dissipation capacity, displacement ductility factor, and stiffness degradation. From the study, the following conclusions were made:

(i) The study affirmed that aspect ratio (t_s/t_w) has a significant effect on the ultimate load capacity and cumulative energy dissipation capacity of RC shear wall-slab connection. As aspect ratio (t_s/t_w) increased from 0.6 to 0.8 and 0.8 to 1.0, the ultimate load capacity increased up to 61.7% and 73.34%, respectively, under different connection types. On the other hand, as the aspect ratio (t_s/t_w) increased from 0.6 to 0.8 and from 0.6 to 1.0, the cumulative energy dissipation capacity increased up to 17.7% and 134.49%, respectively, with the different connection types.

(ii) Aspect ratio (H/W_e) slightly affects the ultimate load capacity of shear wall-slab connection when compared to aspect ratio (t_s/t_w). As the aspect ratio (H/W_e) increases, the ultimate load capacity of the connection increase. The ultimate load resistance of the connection with an aspect ratio (H/W_e) of 1.67 was 1.15% and 1.6% greater than the connection with an aspect ratio (H/W_e) of 1.46 and 1.3, respectively. In addition, the energy dissipation capacity is increased as the aspect ratio (H/W_e) increased.

(iii) As concrete compressive strength increases, the ultimate load capacity and cumulative energy dissipation capacity of shear wall-slab connection also increased.

(iv) The load-carrying capacity and the energy dissipation capacity of RC exterior shear wall-slab connection are slightly affected by connection type when compared to other study parameters.

(v) The ductility of the RC exterior shear wall-slab connection increased as t_s/t_w increased, as H/W_e decreased, and as concrete strength decreased.

(vi) The stiffness of RC exterior shear wall-slab connection decreased as the number of cycles increased. However, the cumulative energy dissipation capacity of the connection increased as the number of cycles increased.

Data Availability

All data are available in the article.

Conflicts of Interest

The authors declare that they have no conflicts of interest regarding the publication of this paper.

Acknowledgments

The authors would like to thank all those who supported them in reviewing the paper.

References

[1] G. S. Pillai, J. Krishnan Prabhakaran, and V. Rajkumar, "Parametric study of exterior shear wall-floor slab connections," *Journal of Performance of Constructed Facilities*, vol. 29, no. 6, Article ID 04014156, 2015.

[2] H. J. Lee and D. A. Kuchma, "Seismic overstrength of shear walls in parking structures with flexible diaphragms," *Journal of Earthquake Engineering*, vol. 11, no. 1, pp. 86–109, 2007.

[3] M. Y. Kaltakci, M. Ozturk, and M. H. Arslan, "An experimental investigation for external RC shear wall applications," *Natural Hazards and Earth System Sciences*, vol. 10, no. 9, pp. 1941–1950, 2010.

[4] A. Gomez-Bernal and H. J. Garcia, "Interaction between shear walls and transfer-slabs , subjected to lateral and vertical loading," in *Proceedings of the Vienna Congress on Recent Advances in Earthquake Engineering and Structural Dynamics 2013 (VEESD 2013)*, vol. 2013, no. 447, pp. 28–30, Vienna Austria, August 2013.

[5] A. A. N. Al-aghbari, S. H. Hamzah, N. H. A. Hamid, and N. A. Rahman, "Structural performance of two types of wall slab connection under out-of-plane lateral cyclic loading," *Journal of Engineering Science & Technology*, vol. 7, no. 2, pp. 177–194, 2012.

[6] S. H. Luk and J. S. Kuang, "Seismic Behaviour of RC Exterior Wide Beam-Column Joints," in *Proceedings of the 15th World Conference on Earthquake Engineering*, Article ID 10987, Lisbon, Portugal, September 2012.

[7] R. Kumar, S. Sidhu, and H. Singh, "Seismic behaviour of shear wall framed buildings," *Int. J. Eng. Technol. Manag. Appl. Sci*, vol. 2, no. 1, pp. 28–38, 2014.

[8] M. Memon, "Wall - slab junction with special shear," in *Proceedings of the 5th Civil. Engineerings. Conference. Asian Region*, Goa, India, August 2010.

[9] M. Chu, L. Jiliang, C. Huichen et al., "Experimental study on seismic behaviors of assembled monolithic concrete shear walls built with precast two-way hollow slabs with various details," *Jianzhu Jiegou Xuebao/Journal Build. Struct*, vol. 35, no. 1, pp. 93–102, 2014.

[10] A. A. Abdul Aziz Ansari, M. A. Muhammad Aslam Bhutto, N. Nadeem-ul-Karim Bhatti, and R. A. Rafique Ahmed Memon, "Strength of Wall-Slab Junction with New Form of Shear Reinforcement in a Laterally Loaded Tall Shear Wall Building," *Journal of Civil Engineering and Architecture*, vol. 9, no. 2, pp. 193–206, 2015.

[11] R. S. Surumi, K. P. Jaya, and S. Greeshma, "Modelling and assessment of shear wall-flat slab joint region in tall structures," *Arabian Journal for Science and Engineering*, vol. 40, no. 8, pp. 2201–2217, 2015.

[12] S. Kaushik and K. Dasgupta, "Seismic damage in shear wall-slab junction in RC buildings," *Procedia Engineering*, vol. 144, pp. 1332–1339, 2016.

[13] S. R. Salim and K. P. Jaya, "Evaluation of Reinforced Concrete Wall – Flat Slab Connection With a Noval Ductile Detailing," in *Proceedings of the 16th World Conf. Earthquake, 16WCEE 2017*, vol. 3236, Santiago, Chile., January 2017.

[14] European Committee for Standardization, *Eurocode 2: Design of concrete structures—Part 1: General rules and rules for buildings*, vol. 1, European Committee for Standardization, Brussels, Europe, 2002.

[15] J. G. Stoner and M. A. Polak, "Finite element modelling of GFRP reinforced concrete beams," *Computers and Concrete*, vol. 25, no. 4, pp. 369–382, 2020.

[16] A. Inc, "ABAQUS Version 6.10-1 Analysis User's Manual," *Dassault Systèmes Simulia Corp*, vol. III, pp. 1–10, 2017.
[17] W. Demin and H. Fukang, "Investigation for plastic damage constitutive models of the concrete material," *Procedia Engineering*, vol. 210, pp. 71–78, 2017.
[18] B. Alfarah, F. López-Almansa, and S. Oller, "New methodology for calculating damage variables evolution in Plastic Damage Model for RC structures," *Engineering Structures*, vol. 132, pp. 70–86, 2017.
[19] Y. Sümer and M. Aktaş, "Defining parameters for concrete damage plasticity model," *Chall. J. strcutural Mech*, vol. 1, no. 3, pp. 149–155, 2015.
[20] T. Wang and T. T. C. Hsu, "Nonlinear finite element analysis of concrete structures using new constitutive models," *Computers & Structures*, vol. 79, no. 32, pp. 2781–2791, 2001.
[21] H. Kupfer, H. Hilsdorf, and H. Rusch, "Behaviour of concrete under biaxial stresses," *ACI J. Proceedings*, vol. 66, no. 8, pp. 656–666, 1969.
[22] J. Lubliner, J. Oliver, S. Oller, and E. Oñate, "A plastic-damage model for concrete," *International Journal of Solids and Structures*, vol. 25, no. 3, pp. 299–326, 1989.
[23] J. Lee, G. L. Fenves, and M. Asce, "Plastic-damage model for cyclic loading of concrete structures," *Journal of Engineering Mechanics*, vol. 124, no. 8, pp. 892–900, 1998.
[24] R. Malm, G. S. James, and S. Hakan, "Monitoring and evaluation of shear crack initiation and propagation in webs of concrete box-girder sections," in *Proceedings of the International Conference on Bridge Engineering - Challenges*, Hong Kong, China, November 2003.
[25] R. Malm, *Predicting Shear Type Crack Initiation and Growth in concrete with Non-linear Finite Element Method*, Thesis for: PhD ThesisAdvisor, KTH, Lindstedtsvägen, Stockholm, 2009.
[26] W. Ren, L. H. Sneed, Y. Yang, and R. He, "Numerical simulation of prestressed precast concrete bridge deck panels using damage plasticity model," *International Journal of Concrete Structures and Materials*, vol. 9, no. 1, pp. 45–54, 2015.
[27] S. Maleki and S. Bagheri, "Behavior of channel shear connectors, Part II: analytical study," *Journal of Constructional Steel Research*, vol. 64, no. 12, pp. 1341–1348, 2008.
[28] A. Feyissa and G. Kenea, "Performance of shear connector in composite slab and steel beam with reentrant and open trough profiled steel sheeting," *Advances in Civil Engineering*, vol. 2022, p. 14, 2022.
[29] J. Zhang, C. Ding, X. Rong, H. Yang, K. Wang, and B. Zhang, "Experimental seismic study of precast hybrid SFC/RC beam-column connections with different connection details," *Engineering Structures*, vol. 208, Article ID 110295, 2020.
[30] M. J. Shannag, N. Abu-Dyya, and G. Abu-Farsakh, "Lateral load response of high performance fiber reinforced concrete beam-column joints," *Construction and Building Materials*, vol. 19, no. 7, pp. 500–508, 2005.
[31] N. Ganesan, P. V. Indira, and R. Abraham, "Steel fibre reinforced high performance concrete beam-column joints subjected to cyclic loading," *ISET Journal of Earthquake Technology*, vol. 44, no. 3–4, pp. 445–456, 2007.